Eur. Phys. J. A **29**, 227–234 (2006)
DOI 10.1140/epja/i2006-10072-2

THE EUROPEAN PHYSICAL JOURNAL A

$\mu_p G_{Ep}/G_{Mp}$ and qF_{2p}/F_{1p} in a relativistic quark model

W.R.B. de Araújo[1], T. Frederico[1,a], M. Beyer[2], and H.J. Weber[3]

[1] Departamento de Física, Instituto Tecnológico de Aeronáutica, Centro Técnico Aeroespacial, 12.228-900 São José dos Campos, São Paulo, Brazil
[2] Fachbereich Physik, Universität Rostock, 18051 Rostock, Germany
[3] Department of Physics, University of Virginia, Charlottesville, VA 22904, USA

Received: 9 March 2006 / Revised: 29 June 2006 /
Published online: 25 August 2006 –
Communicated by A. Schäfer

Abstract. The possible zero of the proton electromagnetic form factor ratio G_{Ep}/G_{Mp} is studied within a light-front quark model. The position of the zero is determined by the presence of a hard constituent quark component in the nucleon wave function. The description of the data for the ratios $\mu_p G_{Ep}/G_{Mp}$ and qF_{2p}/F_{1p} is improved when the hard-scale component of the nucleon wave function is considered.

PACS. 12.39.-x Phenomenological quark models – 13.40.-f Electromagnetic processes and properties – 13.40.Gp Electromagnetic form factors – 14.20.Dh Protons and neutrons

It is a challenge to understand the physical implications of the recent data of the proton electromagnetic form factor ratios extracted from polarization-transfer experiments [1,2], to our present view of nucleon structure. The data for the $\mu_p G_{Ep}/G_{Mp}$ ratio [1,2] shows a strong and almost linear decrease with momentum transfer up to $\sim 6\,[\mathrm{GeV}/c]^2$, while qF_{2p}/F_{1p} presents a plateaux starting at $q^2 \sim 2\,[\mathrm{GeV}/c]^2$.

An important issue in the discussion of the experimental proton form factors is the inconsistence between the ratio G_{Ep}/G_{Mp} extracted from the cross-section using the Rosenbluth separation technique and the one obtained directly from the polarization-transfer data. It is becoming clear that the two-photon exchange process can solve this problem, giving a considerable effect in the Rosenbluth data towards the ratio extracted from polarization-transfer experiments, which only gets a few-percent correction [3–8]. Therefore, the decrease of the proton form factor ratio with momentum is by now not under question.

An extrapolation of the linear decreasing trend of the proton form factor ratio indicates a zero of G_{Ep} for $q^2 \sim 7.7\,[\mathrm{GeV}/c]^2$ [2], which is also incorporated in the new empirical fit of the proton form factors [9].

The extension of the Gari-Krümpelmann model [10] to fit the recent proton data also suggests the presence of a zero of G_{Ep}, although at a higher values of $q^2 \sim 14\,[\mathrm{GeV}/c]^2$. Also, the analysis of the nucleon charge and magnetization using the new data suggested a zero crossing in G_{Ep} near $-q^2 \sim 10\,[\mathrm{GeV}/c]^2$ [11]. Another approach including a phenomenological pion cloud and a quark core in the nucleon presents a G_{Ep} zero around $9\,[\mathrm{GeV}/c]^2$ [12].

The discovery at Jefferson Laboratory, that the ratio qF_{2p}/F_{1p} is approximately constant for $-q^2$ between $2\,[\mathrm{GeV}/c]^2$ and $6\,[\mathrm{GeV}/c]^2$ [1,2], shows that the helicity of the hadron is not conserved in the photon absorption process in contrast to the expectations from perturbative QCD [13,14]. Within relativistic constituent quark models, the qualitative and quantitative aspects of the data were predicted or reproduced by many calculations [15–21], as discussed in detail in the recent review of the nucleon electromagnetic form factors [22]. Light-front relativistic models also leads to a variety of non-spherical shapes in the proton spin-dependent quark densities [23]. It was pointed out in ref. [20] that the constraint of Poincaré invariance within a light-front constituent quark model of the nucleon [24,17] leads to a substantial violation of the helicity conservation rule and consequently to the flattening of qF_{2p}/F_{1p} in the range of momentum transfers of the experiments.

The plateaux of the qF_{2p}/F_{1p} ratio between $2\,[\mathrm{GeV}/c]^2 \lesssim -q^2 \lesssim 6\,[\mathrm{GeV}/c]^2$ corresponds to the decrease of $\mu_p G_{Ep}/G_{Mp}$ and to the extrapolated zero at $-q^2 \sim 7.7\,[\mathrm{GeV}/c]^2$ [2]. The change of sign in G_{Ep} was indeed predicted by three-quark light-front models [17,18,25] and by a point-form constituent quark model [19].

The nucleon light-front model with tunable quark spin couplings from an effective Lagrangian [25] is able to account for the nucleon static properties, while the zero

[a] e-mail: tobias@ita.br

of G_{Ep} appeared at too low values of $-q^2$ between 3 to $4\,[\mathrm{GeV}/c]^2$. Using the Bakamjian-Thomas construction [26] for the spin coupling between the quarks in the nucleon wave function, the zero of G_{Ep} appeared at higher values of $-q^2 \sim 5.5\,[\mathrm{GeV}/c]^2$ [17]. The essential difference between the two calculations resides in the argument of the Melosh rotations [27] in the nucleon wave function, *i.e.*, in Bakamjian-Thomas construction it corresponds to three noninteracting quarks, while in the effective Lagrangian scheme the kinematical quark momentum is constrained by the nucleon momentum [28].

Let us remark, that in the present model the full momentum dependence of each quark is taken into account in the wave function, and it should be distinguished from quark-diquark models, where the diquark is taken as another constituent (see, *e.g.*, [29]). Our nucleon wave function model resembles the one proposed in ref. [30], with the distinctions that we use a completely symmetrical momentum component of the wave function depending only on M_0, and the spin coupling coefficients come from an effective Lagrangian.

The effective Lagrangian approach to the quark spin coupling in the nucleon [25], accounts for the static electromagnetic observables with a totally symmetric momentum component of the wave function, however it has to be improved to be able to describe the new $\mu_p G_{Ep}/G_{Mp}$ data. In this approach, the effective Lagrangian for the N-q coupling is given by

$$\mathcal{L}_{N\text{-}3q} = \alpha\; m_N \epsilon^{lmn} \overline{\Psi}_{(l)} i\tau_2\gamma_5 \Psi^C_{(m)} \overline{\Psi}_{(n)} \Psi_N + (1-\alpha)\epsilon^{lmn} \overline{\Psi}_{(l)} i\tau_2\gamma_\mu\gamma_5 \Psi^C_{(m)} \overline{\Psi}_{(n)} i\partial^\mu \Psi_N + \mathrm{H.C.}, \quad (1)$$

where τ_2 is the isospin matrix, the color indices are $\{l, m, n\}$ and ϵ^{lmn} is the totally antisymmetric symbol. The conjugate quark field is $\Psi^C = C\overline{\Psi}^\top$, where $C = i\gamma^2\gamma^0$ is the charge conjugation matrix; α is a parameter to choose the spin coupling parameterization.

The momentum scale of the nucleon wave function for Gaussian and power law shapes with constituent quark mass of 0.22 GeV, was found in our previous work to be about 0.6–0.8 GeV from the fit of the nucleon magnetic moments and its radius [25]. Also, we observed that the neutron charge form factor constrains the relativistic quark spin coupling scheme, suggesting that the scalar pair ($\alpha = 1$) in the effective Lagrangian is preferred.

However, the effective Lagrangian approach to the quark spin coupling, while it allows a reasonable account of the static electromagnetic nucleon observables with a totally symmetric momentum component of the wave function, has a too small momentum scale which leads to the zero of G_{Ep} at much lower values of q^2 than the experimental data indicates [2,9]. Therefore, within this approach, one is led to introduce another term in the momentum component of the wave function which would represent a higher momentum scale and fit the ratio G_{Ep}/G_{Mp} without changing the conclusions found at low momentum transfers.

In recent works with light-front models [31–33] applied to mesons, a high momentum physical scale appears related to the short-ranged interaction between the constituent quarks. It was found a reasonable description of the meson spectrum and pion properties including a Dirac-delta interaction in the mass-squared operator [31–33], inspired by the hyperfine interaction from the effective one-gluon exchange between the constituent quarks [31, 34]. The model [33] reveals some of the physics contained in the observation of the fact that the trajectories of the mesons in the (n, M^2)-plane are almost linear [35,36]. The model naturally incorporates the small pion mass as a consequence of the short-ranged attraction in the spin-zero channel, which is also responsible for the splitting in the pion and rho-meson mass spectrum [33].

The short-ranged attractive part of the quark-quark interaction, present in the Godfrey and Isgur model [37], generates as well a high momentum component in the light-cone pion wave function above $1\,[\mathrm{GeV}/c]$ and successfully described the electroweak structure of the pion [38]. Nonetheless, it was pointed out that the existing electroweak data was not enough to obtain an unambiguous conclusion about the presence of hard-constituent quarks in the hadron wave function [39]. Recently, this discussion led to a new insight when the valence-quark light-cone momentum distribution was probed in the experiment of diffractive dissociation of $500\,[\mathrm{GeV}/c]$ π^- into dijets [40], which supports the importance of the asymptotic part of the wave function [14] and the presence of a high momentum component in the pion wave function [32].

Motivated by the previous discussion, which indicates the necessity of a strong short-ranged attractive interaction in the spin-zero channel, and a high momentum tail in the pion valence component, we also introduce a high momentum tail in the valence component of the nucleon wave function and test it in our calculation of the form factors. Indeed, the quality of the model results in respect to the new data for the $\mu_p G_{Ep}/G_{Mp}$ ratio improves substantially, as we will show.

The constituent quark is a complex degree of freedom which includes the physics of an infinite number of Fock states of the fundamental theory, as it comes from the nonperturbative quark dressing. At low momentum the constituent quark, as a collective degree of freedom, is subject to soft physics and its properties should evolve with momentum and asymptotically to the current quark ones. The strong interaction dresses nonperturbatively the quark giving a nontrivial structure to the constituent quark. For example, in the study performed by ref. [41] for light mesons, it was used a rainbow truncation of the Schwinger-Dyson equations combined with the ladder Bethe-Salpeter which implied in a dressed quark-photon vertex and a running quark mass. The nontrivial constituent quark structure was also necessary to be considered in phenomenological studies of the electromagnetic structure of the nucleon, through a constituent quark form factor [42,43].

Therefore, two main effects should be in principle considered in the model: the running quark mass and the constituent quark form factor. As the constituent quark mass in our model is already pretty small (0.22 GeV) and

in principle it should decrease by increasing the momentum, the nonconstant behavior will not have an important impact in the form factors as the average momentum of the quarks increases. We believe that the decrease of the constituent quark mass for higher momentum will have no major effect in our calculations, because the momentum terms are dominant in the form factors as well as in the momentum component of the wave function (the quark mass appears through M_0, the free mass of the three-quark system, see eq. (2)). However, the constituent quark form factor cannot be neglected and it will be considered in our calculations of the nucleon electromagnetic form factors.

Our aim in this work is to study the performance of a two-scale shape of the momentum component of the wave function in a light-front model in which an effective Lagrangian construction of the spin coupling between the quarks, eq. (1), with a scalar form is used. The scalar form of the coupling is chosen to allow a simultaneous reproduction of the magnetic moment and electric form factor of the neutron [25].

We choose a simple two-term power law shape [44,34] for the momentum component of the nucleon wave function without a node, written as

$$\Psi_{\rm Power}\big(M_0^2\big) = N_{\rm Power}\left[\left(\frac{1+M_H^2/\beta^2}{1+M_0^2/\beta^2}\right)^p + \left(\frac{1+M_H^2/\beta_1^2}{1+M_0^2/\beta_1^2}\right)^p\right], \qquad (2)$$

which presents an asymptotic behavior as suggested by QCD. The normalization is determined by the proton charge. The width parameters, *i.e.*, the characteristic momentum scales of the wave function are β and β_1, while M_0 is the free mass of the three-quark system (see eq. (A.8)). The lower momentum scale is essentially determined by the static nucleon observables and the higher one is related to the zero of G_{Ep}. The mass scale parameter M_H gives the large value of M_0 at which the two terms of eq. (2) are equal. The parameter M_H can be interpreted as a reference value of the free mass of the three-quark system for which the second term of eq. (2) is important. Note that the asymptotic behavior of eq. (2) does not depend on the particular values of the parameters. The totally symmetric forms of eq. (2), due the relativistic spin coupling coefficients which depend on momentum, effectively lead to the breaking of the $SU(6)$ flavor symmetry as discussed in ref. [18].

The power law fall-off from general QCD perturbative arguments has a value of $p = 3.5$ in eq. (2) [44,34]. From the point of view of the static electroweak observables, the value of p does not present an independent feature, once one static observable is fitted, the other is strongly correlated as long as $p > 2$ [25,44]. Here, we choose for our calculations $p = 3$. Note that the power law wave function was predicted in QCD by counting rules taking into account the exchange of hard gluons between the quarks, but it was applied in the study of the static electroweak properties of the proton [44,34] producing essentially the same results as a Gaussian wave function [25]. Although the power law wave function is justified in QCD by hard physics, it appears to work phenomenologically at low momentum. This occurs due to the choice of the M_0-dependence in the power law form, which for small values of M_0 cannot be distinguished from a commonly used Gaussian wave function.

The light-front formulation of the nucleon electroweak form factors from ref. [25] uses the effective Lagrangian, eq. (1), to construct the coupling of the quark spin in the valence component of the wave function. The form factor calculation begins with the impulse approximation defined within covariant field theory. The nucleon virtual photon absorption amplitude is projected on the three-dimensional hypersurface, $x^+ = x^0 + x^3 = 0$, (see, *e.g.*, ref. [45]). The elimination of the relative light-front time between the particles in favor of the global time propagation [46] comes from the analytical integration in the individual light-front energies ($k^- = k^0 - k^3$) in the two-loop amplitude. Then, the momentum component of the nucleon light-front wave function is introduced into the remaining form of the two-loop three-dimensional momentum integrations which define the matrix elements of the electroweak current [25,47,48].

The plus component of the nucleon current ($J_N^+ = J_N^0 + J_N^3$) for momentum transfers satisfying the Drell-Yan condition $q^+ = q^0 + q^3 = 0$ is used to obtain the electromagnetic form factors. The contribution of the Z-diagram is minimized in a Drell-Yan reference frame, while the wave function contribution to the current is maximized [34,45,47–49]. We use the Breit frame, where the four-momentum transfer $q = (0, \vec{q}_\perp, 0)$ is such that $(q^+ = 0)$ and $\vec{q}_\perp = (q^1, q^2)$, satisfying the Drell-Yan condition.

The nucleon electromagnetic form factors are calculated with the matrix elements of the current $J_N^+(q^2)$ in the light-front spinor basis in the Breit frame with the Drell-Yan condition [15,25]. The Dirac and Pauli form factors are, respectively, given by

$$F_{1N}\big(q^2\big) = \frac{1}{\sqrt{1+\eta}}\langle\uparrow|J_N^+\big(q^2\big)|\uparrow\rangle,$$
$$F_{2N}\big(q^2\big) = \frac{1}{\sqrt{\eta}\sqrt{1+\eta}}\langle\uparrow|J_N^+\big(q^2\big)|\downarrow\rangle, \qquad (3)$$

where $\eta = -q^2/4m_N$. The momentum transfer in the Breit frame was chosen along the x-direction, *i.e.*, $\vec{q}_\perp = (\sqrt{-q^2}, 0)$.

The nucleon electric and magnetic form factors (Sachs form factors) are given by

$$G_{EN}\big(q^2\big) = F_{1N}\big(q^2\big) + \frac{q^2}{4m_N^2}F_{2N}\big(q^2\big),$$
$$G_{MN}\big(q^2\big) = F_{1N}\big(q^2\big) + F_{2N}\big(q^2\big), \qquad (4)$$

where $N = n$ or p. $\mu_N = G_{MN}(0)$ is the magnetic moment and $\kappa_N = F_{2N}(0)$ is the anomalous one. The charge mean square radius is $r_N^2 = 6\frac{{\rm d}G_{EN}(q^2)}{{\rm d}q^2}|_{q^2=0}$.

The microscopic matrix elements of the nucleon electromagnetic current are derived from the effective Lagrangian, eq. (1), within the light-front impulse approximation which is represented by the four three-dimensional

Table 1. Nucleon electromagnetic static observables and zero of $G_{Ep}(q^2)$ for one- and two-scale models. The momentum scale parameters of the two terms of the wave function, eq. (2), are shown in the first, second and third columns, respectively. The proton and neutron magnetic moments and mean square radii, are presented in the fourth through seventh columns. In the last column the square momentum transfer at which $G_{Ep}(q_0^2) = 0$ is shown. The references for the experimental values are given in the table.

β [GeV]	β_1 [GeV]	M_H [GeV]	μ_p [μ_N]	r_p^2 [fm]^2	μ_n [μ_N]	r_n^2 [fm]^2	q_0^2 [GeV/c]^2
0.396	10.56	5.92	3.07	1.09	-1.89	-0.07	9.04
0.447	–	–	3.11	1.06	-1.91	-0.08	3.28
Expt.	–	–	2.79	0.66 ± 0.06 [50] 0.74 ± 0.02 [51] 0.77 ± 0.03 [52]	-1.91	-0.113 ± 0.005 [53]	~ 7.7

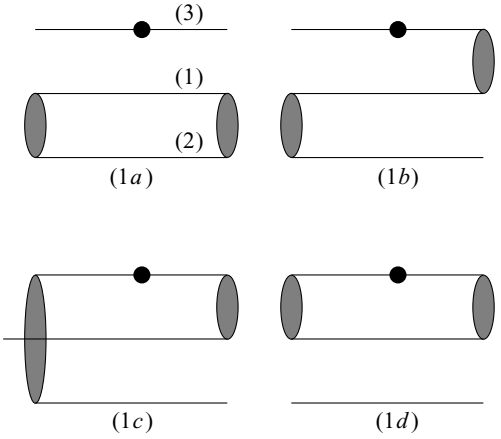

Fig. 1. Diagrammatic representation of the nucleon photoabsorption amplitude. The gray blob represents the spin invariant for the coupled quark pair in the effective Lagrangian, eq. (1). The black circle in the fermion line represents the action of the current operator on the quark.

two-loop diagrams of fig. 1 [25], which embodies the antisymmetrization of the quark state in the wave function. The matrix elements of the electromagnetic current are calculated considering only the process on quark 3, due to the symmetrization of the microscopic matrix element after the factorization of the color degree of freedom. Therefore, the microscopic operator of the nucleon electromagnetic current is the sum of each amplitude represented by the diagrams (1a) to (1d):

$$J_N^+(q^2) = J_{aN}^+(q^2) + 4J_{bN}^+(q^2) + 2J_{cN}^+(q^2) + 2J_{dN}^+(q^2) \quad (5)$$

with the appropriate statistical factors, from the identity of quarks 1 and 2. Another factor of 2 multiplies J_{bN}^+ due to the exchange between the pairs in the initial and final nucleons, which gives the same matrix element as a consequence of time reversal and parity transformation properties. The expressions of the microscopic matrix elements of the plus component of the current are presented in detail in the appendix, following closely ref. [25].

In this work, we perform calculations with the scalar coupling $\alpha = 1$ in the effective Lagrangian, eq. (1). It corresponds to the spin coupling coefficients in which the Melosh rotations of the quark spin have the arguments defined by the kinematical momentum of the quarks in pair and in the nucleon rest frames constrained by the total momentum [28], while in the Bakajmian-Thomas construction the argument of the Melosh rotations is defined in the rest frame of three free particles.

The relativistic model of the nucleon adopted here assumes the dominance of the valence component in the wave function and in the computation of the static electromagnetic observables and form factors. Therefore, the results are strongly constrained and essentially the general features found in our calculations are independent of the detailed shape of the wave function, but of course depend on the momentum scales in eq. (2). In the numerical evaluation of the form factors, we use a constituent quark mass value of $m = 0.22\,\mathrm{GeV}$ [25,38].

A single scale light-front wave function, Gaussian or power law, with momentum scale parameter adjusted from the fit of the neutron or proton magnetic moment, is known to have a reasonable proton charge radius, due to the strong correlation between these observables [44,34, 25]. However, the zero of G_{Ep} appears at too low squared momentum transfer, q_0^2 between 3-4 $[\mathrm{GeV}/c]^2$. When we attempt to fit q_0^2 to values around 8 $[\mathrm{GeV}/c]^2$ by increasing the momentum scale in the Gaussian and power law wave functions, we find an unreasonably small proton size and consequently wrong magnetic moments as well, which leave no room for improvements in the framework of those one-scale models.

By introducing a two-scale power law momentum component of the wave function in the calculation with scalar coupling, we are able to get a reasonable description of both the nucleon static observables and the zero of G_{Ep}, as shown in table 1. We have also considered a constituent quark form factor which produces a quark radius of 0.18 fm, within the values suggested by ref. [43]. A dipole form factor was chosen,

$$f_q(q^2) = \frac{1}{\left(1 - \frac{q^2}{\gamma}\right)^2} \quad (6)$$

with $\gamma = 14\,[\mathrm{GeV}/c]^2$ and no anomalous magnetic moment for the constituent quark. The value of γ was

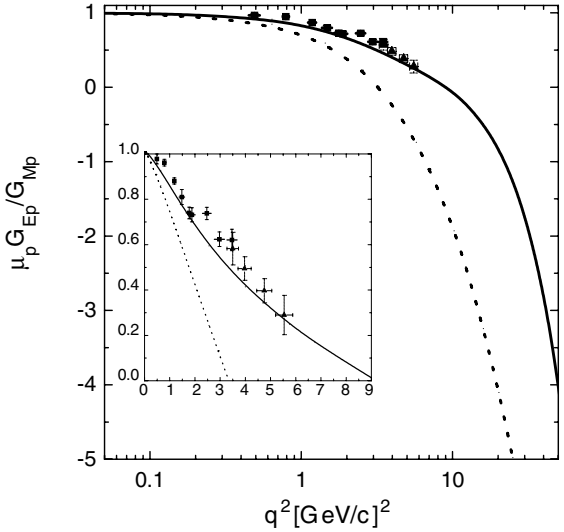

Fig. 2. Proton form factor ratio. Results for the two-scale wave function (solid line) and one-scale model (dashed line). The inset magnifies the plot up to $9\,[\mathrm{GeV}/c]^2$. Experimental data from refs. [1] (squares) and [2] (triangles).

strongly constrained by the fit of the proton magnetic form factor for momentum transfers above few GeV.

The scalar coupling provides the best agreement with the neutron radius, when the neutron magnetic moment is fitted [25]. We have chosen to fit the neutron magnetic moment due to the strong sensitivity of G_{En} to its value [25]. The high momentum scale $M_H \sim 6\,\mathrm{GeV}$, should be understood as a reference value and we point out that we cannot exclude lower values for M_H, and indeed the effect of the new parameterization is seen at lower momentum transfer scales.

In fig. 2, we show the results for the proton $\mu_p G_{Ep}(q^2)/G_{Mp}(q^2)$ ratio for the scalar model. From table 1 one could anticipate the results we found. Reasonable agreement with the data [1,2] is seen for the two-scale model which has the zero of $G_{Ep}(q^2)$ around the suggested experimental value of $7.7\,[\mathrm{GeV}/c]^2$. Due to the same asymptotic behavior of the wave function, we find that the one-scale and two-scale models predict a similar strong decrease in the form factor ratio with increasing momentum transfers.

The calculations for the proton $qF_{2p}(q^2)/\kappa_p F_{1p}(q^2)$ ratio are shown in fig. 3. The one-scale model fails completely to describe the experimental data, while a reasonable agreement with the data [1,2] is seen for the two-scale model. As expected, with increasing momentum the results for the two-scale model tend to show the same behavior as for the one-scale model. (Fine tuning could delay a little the increase of $qF_{2p}(q^2)/\kappa_p F_{1p}(q^2)$ ratio). The proton magnetic form factor distinguishes both parameterizations, the two-scale model exhibits a slower decrease than the one-scale model above 2–3 $[\mathrm{GeV}/c]$.

Figure 4 shows the neutron form factors. The electric form factor in both models are qualitatively consistent with the data. Also both agree below $9\,[\mathrm{GeV}/c]^2$ consistent with the onset of the high momentum scale.

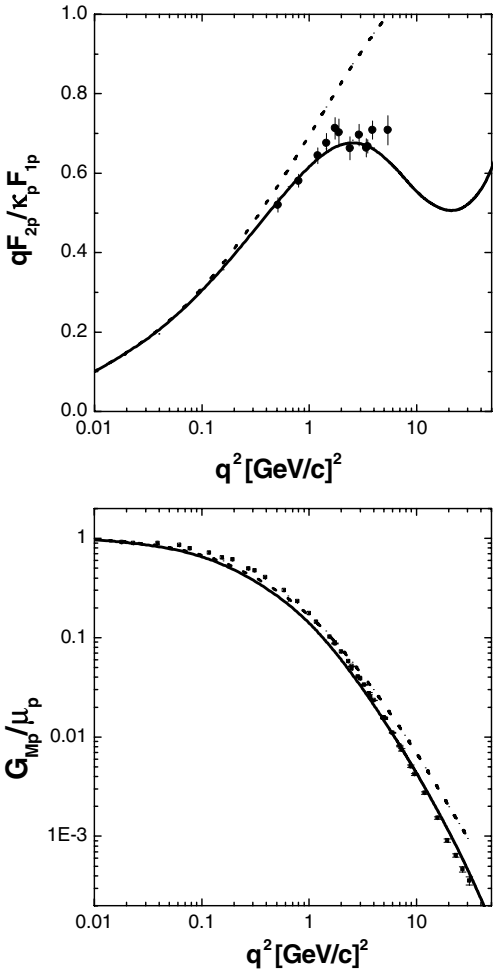

Fig. 3. Proton form factor ratio $qF_{2p}(q^2)/\kappa_p F_{1p}(q^2)$ and magnetic form factor. Curves labeled as in fig. 2. The experimental data presented in the top and bottom frames are taken from refs. [1,2] and from the compilation of ref. [22], respectively.

The magnetic form factor has a zero for the two-scale model while the one-scale model exhibits a monotonic decrease with momentum transfer. The results for G_{Mn} below $3\,[\mathrm{GeV}/c]^2$ do not depend on the model as μ_n for both calculations are quite near (see table 1).

In summary, we have shown that it is reasonable to expect that two-scale wave function models of eq. (2) parameterize the lowest Fock state component of the nucleon light-front wave function. Within effective models inspired by QCD, the interaction between the constituent quarks in the squared-mass operator has an attractive short-ranged component in the scalar channel. The valence component of a wave function is an eigenstate of an effective mass operator equation for constituent quark degrees of freedom, in which the effective interaction contains in principle all the complexity of QCD [31,34]. In general, an attractive short-ranged interaction will produce a high momentum component in the wave function, which gives physical meaning to the present two-scale model.

We show how to improve the nucleon light-front model based on an effective Lagrangian approach to the spin cou-

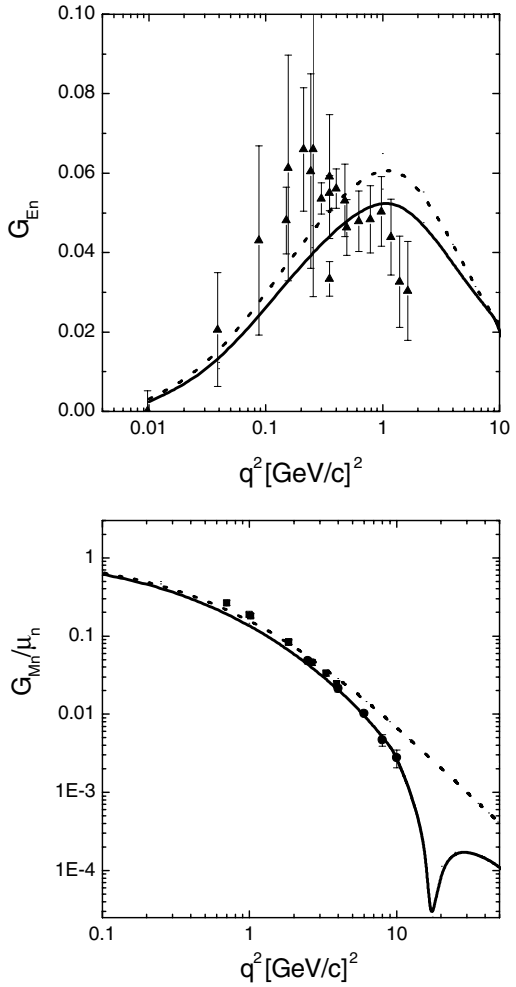

Fig. 4. Neutron electromagnetic form factors. Curves labeled as in fig. 2. Triangles are the experimental data taken from the compilation of ref. [22]; square and circles are the data from refs. [54] and [55], respectively.

pling of the quarks by introducing a physically motivated two-scale wave function. The model improves the description of the present data of the proton form factors ratios and static properties, as well as the neutron form factor data. The importance of the spin coupling scheme for the neutron electric form factor found for the two-scale model is consistent with previous results [25]. Pionic cloud effects and Poincarè invariance [21], produces results for the neutron electric form factor similar to ours. This may imply that to some extent, pionic effects are partially included by our parameterization. The hard momentum scale is strongly related to the position of the G_{Ep} zero. The zero in the magnetic neutron form factor is related to the hard scale and the scalar coupling form. The present data for the proton form factor ratios suggests a hard momentum scale of about 6 [GeV/c].

WRBA thanks FAPESP (Fundaşcão de Amparo à Pesquisa do Estado de São Paulo) for financial support. TF thanks CNPq (Conselho Nacional de Pesquisas) and FAPESP. We thank CAPES/DAAD for partial financial support. We also thank CENAPAD/UNICAMP and LCCA/USP for providing computational facilities.

Appendix A. Matrix elements of the microscopic current

The derivation of the matrix elements of the microscopic nucleon current operator composed by $J^+_{\beta N}$, $\beta = a, b, c, d$ of eq. (5) in terms of the valence nucleon wave function follows closely ref. [25]. They are represented by the Feynman diagrams of fig. 1. Note that the blobs in the figure represent the color anti-triplet coupling of a pair of quark fields in scalar-isocalar $(\epsilon^{lmn}\overline{\Psi}_{(l)}i\tau_2\gamma_5\Psi^C_{(m)})$ or vector-isoscalar combination $(\epsilon^{lmn}\overline{\Psi}_{(l)}i\tau_2\gamma_\mu\gamma_5\Psi^C_{(m)})$, from the effective Lagrangian of eq. (1).

The integrations over the minus component of the momentum will be performed to eliminate the relative light-front time in the intermediate-state propagations [46]. This procedure allows to introduce the momentum component of the valence light-front wave function in the computation of form factors (see [47]).

The nucleon electromagnetic current J^+_N derived from the effective Lagrangian has contribution from each photo-absorption amplitude given by the Feynman two-loop triangle diagrams of figs. 1a to 1d. The matrix elements of the current are evaluated between light-front spinor states:

$$u(p,s) = \frac{\not{p} + m_N}{2\sqrt{p^+ m_N}}\gamma^+\gamma^0 \begin{pmatrix} \chi^{\text{Pauli}}_s \\ 0 \end{pmatrix}. \tag{A.1}$$

The photon is absorbed by quark 3, and the diagram of fig. 1a corresponds to

$$\begin{aligned}\langle s'|J^+_{aN}(q^2)|s\rangle &= -\langle N|\hat{Q}_q|N\rangle\,\mathrm{Tr}[i\tau_2(-i)\tau_2]\\ &\times\int\frac{\mathrm{d}^4k_1\mathrm{d}^4k_2}{(2\pi)^8}\Lambda(k_i,p')\Lambda(k_i,p)\bar{u}(p',s')S(k'_3)\gamma^+\\ &\times S(k_3)u(p,s)\,\mathrm{Tr}\Big[S(k_2)\left(\alpha m_N + (1-\alpha)\not{p}\right)\\ &\times\gamma^5 S_c(k_1)\gamma^5\left(\alpha m_N + (1-\alpha)\not{p}'\right)\Big]\end{aligned} \tag{A.2}$$

with $S(p) = \frac{1}{\not{p}-m+i\epsilon}$, and $S_c(p) = [\gamma^0\gamma^2\frac{1}{\not{p}-m+i\epsilon}\gamma^0\gamma^2]^\top$. The four-momentum of the virtual quark 3 after the photo-absorption process is $k'_3 = k_3 + Q$. The matrix element of the quark charge operator in isospin space is $\langle N|\hat{Q}_q|N\rangle$. The function $\Lambda(k_i,p)$ is chosen to introduce the momentum part of the three-quark light-front wave function, after the integrations over k^- are performed. The contribution to the electromagnetic current represented by fig. 1b is given by

$$\begin{aligned}\langle s'|J^+_{bN}(q^2)|s\rangle &= -\langle N|\hat{Q}_q|N\rangle\\ &\times\int\frac{\mathrm{d}^4k_1\mathrm{d}^4k_2}{(2\pi)^8}\Lambda(k_i,p')\Lambda(k_i,p)\bar{u}(p',s')S(k'_3)\gamma^+S(k_3)\\ &\times\left(\alpha m_N + (1-\alpha)\not{p}\right)\gamma^5 S_c(k_1)\gamma^5\\ &\times\left(\alpha m_N + (1-\alpha)\not{p}'\right)S(k_2)u(p,s).\end{aligned} \tag{A.3}$$

The contribution to the electromagnetic current represented by fig. 1c is given by

$$\langle s'|J^+_{cN}(q^2)|s\rangle = \langle N|\tau_2\hat{Q}_q\tau_2|N\rangle \times \int \frac{\mathrm{d}^4k_1\mathrm{d}^4k_2}{(2\pi)^8}\Lambda(k_i,p')\Lambda(k_i,p)\bar{u}(p',s')S(k_1) \times (\alpha m_N + (1-\alpha)\not{p})\,\gamma^5 S_c(k_3)\gamma^+ S_c(k_3')\gamma^5 \times(\alpha m_N + (1-\alpha)\not{p}')S(k_2)u(p,s). \quad (A.4)$$

The contribution to the electromagnetic current represented by fig. 1d is given by

$$\langle s'|J^+_{dN}(q^2)|s\rangle = -\,\mathrm{Tr}\left[\hat{Q}_q\right] \times \int \frac{\mathrm{d}^4k_1\mathrm{d}^4k_2}{(2\pi)^8}\Lambda(k_i,p')\Lambda(k_i,p)\bar{u}(p',s')S(k_2)u(p,s) \times \mathrm{Tr}\left[\gamma^5(\alpha m_N + (1-\alpha)\not{p}')S(k_3')\gamma^+ S(k_3) \times (\alpha m_N + (1-\alpha)\not{p})\,\gamma^5 S_c(k_1)\right]. \quad (A.5)$$

The light-front coordinates are defined as $k^+ = k^0 + k^3$, $k^- = k^0 - k^3$, $k_\perp = (k^1, k^2)$. In each term of the nucleon current, from J^+_{aN} to J^+_{dN}, the Cauchy integrations over k_1^- and k_2^- are performed. That means the on-mass-shell pole of the Feynman propagators for the spectator particles 1 and 2 of the photon absorption process are taken into account. In the Breit frame with $q^+ = 0$ there is a maximal suppression of light-front Z-diagrams in J^+ [47,48]. Thus the components of the momentum k_1^+ and k_2^+ are bounded such that $0 < k_1^+ < p^+$ and $0 < k_2^+ < p^+ - k_1^+$. The four-dimensional integrations of eqs. (A.2) to (A.5) are reduced to the three-dimensional ones of the null plane.

After the integrations over the light-front energies the momentum part of the wave function is introduced into the microscopic matrix elements of the current by the substitution [25,47]:

$$\frac{1}{2(2\pi)^3}\frac{\Lambda(k_i,p)}{m_N^2 - M_0^2} \to \Psi(M_0^2). \quad (A.6)$$

Further, the same momentum component of the wave function is chosen for all N-q coupling schemes for simplification. Note, that the mixed ($\alpha = 1/2$) case could have different momentum dependences for each spin coupling, however, we choose the same momentum functions just to keep contact to the BT approach.

The analytical integration of eq. (A.2) of the k^- components of the momenta yields

$$\langle s'|J^+_{aN}(q^2)|s\rangle = 2p^{+2}\langle N|\hat{Q}_q|N\rangle \times \int \frac{\mathrm{d}^2k_{1\perp}\mathrm{d}k_1^+\mathrm{d}^2k_{2\perp}\mathrm{d}k_2^+}{k_1^+k_2^+k_3^{+2}}\theta(p^+ - k_1^+)\theta(p^+ - k_1^+ - k_2^+) \times \mathrm{Tr}\left[(\not{k}_2+m)(\alpha m_N+(1-\alpha)\not{p})\,(\not{k}_1+m)\left(\alpha m_N+(1-\alpha)\not{p}'\right)\right] \times \bar{u}(p',s')(\not{k}_3'+m)\gamma^+(\not{k}_3+m)u(p,s)\Psi(M_0'^2)\Psi(M_0^2), \quad (A.7)$$

where $k_1^2 = m^2$ and $k_2^2 = m^2$. The free three-quark squared mass is defined by

$$M_0^2 = p^+\left(\frac{k_{1\perp}^2+m^2}{k_1^+} + \frac{k_{2\perp}^2+m^2}{k_2^+} + \frac{k_{3\perp}^2+m^2}{k_3^+}\right) - p_\perp^2, \quad (A.8)$$

and $M_0'^2 = M_0^2(k_3 \to k_3', \vec{p}_\perp \to \vec{p}_\perp')$.

The other terms of the nucleon current, as given by eqs. (A.3)-(A.5) are also integrated over the k^- momentum components of particles 1 and 2 following the same steps used to obtain eq. (A.7) from eq. (A.2):

$$\langle s'|J^+_{bN}(q^2)|s\rangle = p^{+2}\langle N|\hat{Q}_q|N\rangle \times \int \frac{\mathrm{d}^2k_{1\perp}\mathrm{d}k_1^+\mathrm{d}^2k_{2\perp}\mathrm{d}k_2^+}{k_1^+k_2^+k_3^{+\,2}}\theta(p^+ - k_1^+)\theta(p^+ - k_1^+ - k_2^+) \times \bar{u}(p',s')(\not{k}_3'+m)\gamma^+(\not{k}_3+m)\,(\alpha m_N+(1-\alpha)\not{p})\,(\not{k}_1+m) \times(\alpha m_N+(1-\alpha)\not{p}')(\not{k}_2+m)u(p,s)\Psi(M_0'^2)\Psi(M_0^2), \quad (A.9)$$

$$\langle s'|J^+_{cN}(q^2)|s\rangle = p^{+2}\langle N|\tau_2\hat{Q}_q\tau_2|N\rangle \times \int \frac{\mathrm{d}^2k_{1\perp}\mathrm{d}k_1^+\mathrm{d}^2k_{2\perp}\mathrm{d}k_2^+}{k_1^+k_2^+k_3^{+\,2}}\theta(p^+ - k_1^+)\theta(p^+ - k_1^+ - k_2^+) \times \bar{u}(p',s')(\not{k}_1+m)\,(\alpha m_N+(1-\alpha)\not{p})\,(\not{k}_3+m)\gamma^+(\not{k}_3'+m) \times(\alpha m_N+(1-\alpha)\not{p}')(\not{k}_2+m)u(p,s)\Psi(M_0'^2)\Psi(M_0^2), \quad (A.10)$$

$$\langle s'|J^+_{dN}(q^2)|s\rangle = p^{+2}\,\mathrm{Tr}\left[\hat{Q}_q\right] \times \int \frac{\mathrm{d}^2k_{1\perp}\mathrm{d}k_1^+\mathrm{d}^2k_{2\perp}\mathrm{d}k_2^+}{k_1^+k_2^+k_3^{+\,2}}\theta(p^+ - k_1^+)\theta(p^+ - k_1^+ - k_2^+) \times \mathrm{Tr}\left[(\alpha m_N + (1-\alpha)\not{p}')\,(\not{k}_3'+m)\gamma^+ \times(\not{k}_3+m)\,(\alpha m_N+(1-\alpha)\not{p})\,(\not{k}_1+m)\right] \times \bar{u}(p',s')(\not{k}_2+m)u(p,s)\Psi(M_0'^2)\Psi(M_0^2). \quad (A.11)$$

The normalization is chosen such that the proton charge is unity.

References

1. Jefferson Lab Hall A Collaboration (M.K. Jones *et al.*), Phys. Rev. Lett. **84**, 1398 (2000).
2. O. Gayou *et al.*, Phys. Rev. Lett. **88**, 092301 (2002).
3. P.A.M. Guichon, M. Vanderhaeghen, Phys. Rev. Lett. **91**, 142303 (2003).
4. P.G. Blunden, W. Melnitchouk, J.A. Tjon, Phys. Rev. Lett. **91**, 142304 (2003).
5. C.E. Hyde-Wright, K. de Jager, Annu. Rev. Nucl. Part. Sci. **54**, 217 (2004).
6. Y.-C. Chen, A. Afanasev, S.J. Brodsky, C.E. Carlson, M. Vanderhaeghen, Phys. Rev. Lett. **93**, 122301 (2004).
7. S. Kondratyuk, P.G. Blunden, W. Melnitchouk, J.A. Tjon, Phys. Rev. Lett. **95**, 172503 (2005).
8. P.G. Blunden, W. Melnitchouk, J.A. Tjon, Eur. Phys. J. A **24**, 59 (2005).

9. E.J. Brash, A. Koslov, Sh. Li, G.M. Huber, Phys. Rev. C **65**, 051001(R) (2002).
10. E.L. Lomon, Phys. Rev. C **66**, 045501 (2002).
11. J.J. Kelly, Phys. Rev. C **66**, 065203 (2002).
12. J. Friedrich, Th. Walcher, Eur. Phys. J. A **17**, 607 (2003).
13. A.H. Mueller, Phys. Rep. **73**, 237 (1981).
14. G.P. Lepage, S.J. Brodsky, Phys. Rev. D **22**, 2157 (1980).
15. P.L. Chung, F. Coester, Phys. Rev. D **44**, 229 (1991).
16. F. Cardarelli, E. Pace, G. Salmè, S. Simula, Phys. Lett. B **357**, 267 (1995); Few-Body Syst. Suppl. **8**, 345 (1995).
17. M.R. Frank, B.K. Jennings, G.A. Miller, Phys. Rev. C **54**, 920 (1996).
18. F. Cardarelli, S. Simula, Phys. Rev. C **62**, 065201 (2000); S. Simula, nucl-th/0105024.
19. R.F. Wagenbrunn, S. Boffi, W. Klink, W. Plessas, M. Radici, Phys. Lett. B **511**, 33 (2001).
20. G.A. Miller, M.R. Frank, Phys. Rev. C **65**, 065205 (2002).
21. G.A. Miller, Phys. Rev. C **66**, 032201(R) (2002).
22. H. Gao, Int. J. Mod. Phys. E **12**, 1 (2003) and references therein.
23. G.A. Miller, Phys. Rev. C **68**, 022201(R) (2003).
24. F. Schlumpf, Phys. Rev. D **47**, 4114 (1993).
25. W.R.B. de Araújo, E.F. Suisso, T. Frederico, M. Beyer, H.J. Weber, Phys. Lett. B **478**, 86 (2000); E.F. Suisso, W.R.B. de Araújo, T. Frederico, M. Beyer, H.J. Weber, Nucl. Phys. A **694**, 351 (2001).
26. B. Bakamjian, L.H. Thomas, Phys. Rev. **92**, 1300 (1953).
27. H.J. Melosh, Phys. Rev. D **9**, 1095 (1974).
28. W.R.B. de Araújo, T. Frederico, M. Beyer, H.J. Weber, J. Phys. G **25**, 1589 (1999).
29. P. Kroll, M. Schurmann, W. Schweiger, Z. Phys. A **338**, 339 (1991).
30. J. Bolz, P. Kroll, Z. Phys. A **356**, 327 (1996).
31. H.-C. Pauli, Eur. Phys. J. C **7**, 289 (1998); *DLCQ and the effective interactions in hadrons*, in *New Directions in Quantum Chromodynamics*, edited by C.-R. Ji, D.P. Min (American Institute of Physics, 1999) pp. 80-139.
32. T. Frederico, H.C. Pauli, Phys. Rev. D **64**, 054007 (2001).
33. T. Frederico, H.C. Pauli, S.G. Zhou, Phys. Rev. D **66**, 054007; 116011 (2002).
34. S.J. Brodsky, H.-C. Pauli, S.S. Pinsky, Phys. Rep. **301**, 299 (1998) and references therein.
35. F. Iachello, N.C. Mukhpadhyay, L. Zang, Phys. Rev. D **44**, 88 (1991).
36. A.V. Anisovich, V.V. Anisovich, A.V. Sarantesev, Phys. Rev. D **62**, 051502(R) (2000).
37. S. Godfrey, N. Isgur, Phys. Rev. D **32**, 189 (1985).
38. F. Cardarelli, I.L. Grach, I.M. Narodetskii, E. Pace, G. Salmè, S. Simula, Phys. Lett. B **332**, 1 (1994); F. Cardarelli, I.L. Grach, I.M. Narodetskii, G. Salmè, S. Simula, Phys. Lett. B **349**, 393 (1995).
39. H.-M. Choi, C.-R. Ji, Phys. Rev. D **59**, 074015 (1999); D. Arndt, C.-R. Ji, Phys. Rev. D **60**, 094020 (1999).
40. E.M. Aitala *et al.*, Phys. Rev. Lett. **86**, 4768 (2001).
41. P. Maris, P.C. Tandy, Phys. Rev. C **61**, 045202 (2000); P. Maris, C.D. Roberts, Int. J. Mod. Phys. E **12**, 297 (2003); P. Maris, P.C. Tandy, nucl-th/0511017.
42. F. Cardarelli, E. Pace, G. Salme, S. Simula, Phys. Lett. B **357**, 267 (1995).
43. R. Petronzio, S. Simula, G. Ricco, Phys. Rev. D **67**, 094004 (2003); **68**, 099901 (2003)(E).
44. S.J. Brodsky, F. Schlumpf, Phys. Lett. B **329**, 111 (1994); Prog. Part. Nucl. Phys. **34**, 69 (1995).
45. J. Carbonell, B. Desplanques, V. Karmanov, J.-F. Mathiot, Phys. Rep. **300**, 215 (1998) and references therein.
46. J.H.O. Sales, T. Frederico, B.V. Carlson, P.U. Sauer, Phys. Rev. C **61**, 044003 (2000); **63**, 064003 (2001).
47. T. Frederico, G.A. Miller, Phys. Rev. D **45**, 4207 (1992).
48. J.P.B.C. de Melo, H.W. Naus, T. Frederico, Phys. Rev. C **59**, 2278 (1999).
49. B.L.G. Bakker, H.-M. Choi, C.-R. Ji, Phys. Rev. D **63**, 074014 (2001).
50. S.J. Brodsky, J.R. Primack, Ann. Phys. (N.Y.) **52**, 315 (1969).
51. J.J. Murphy II, Y.M. Shin, D.M. Skopik, Phys. Rev. C **9**, 3125 (1974).
52. R. Rosenfelder, Phys. Lett. B **479**, 381 (2000).
53. S. Kopecky *et al.*, Phys. Rev. Lett. **74**, 2427 (1995).
54. G. Holer *et al.*, Nucl. Phys. B **144**, 505 (1976).
55. S. Rock *et al.*, Phys. Rev. Lett. **49**, 1139 (1982).